

# Residual Stress Characterization in a Dissimilar Metal Weld Nuclear Reactor Piping System Mock Up

Matthew Kerr<sup>1,2</sup>

US Nuclear Regulatory Commission  
Office of Nuclear Regulatory Research,  
Washington, DC

Michael B Prime, Hunter Swenson, Miles A Buechler,  
Michael Steinzig

W-13, Los Alamos National Lab, Los Alamos, NM

Bjorn Clausen, Thomas Sisneros

Los Alamos Neutron Science Center  
Los Alamos Nation Lab, Los Alamos, NM

## ABSTRACT

Time-of-flight neutron diffraction, contour method, and surface hole drilling residual stress measurements were conducted at Los Alamos National Lab (LANL) on a lab sized plate specimen (P4) from Phase 1 of the joint U.S. Nuclear Regulatory Commission and Electric Power Research Institute Weld Residual Stress (NRC/EPRI WRS) program. The specimen was fabricated from a 304L stainless steel plate containing a seven pass Alloy 82 groove weld, restrained during welding and removed from the restraint for residual stress characterization. This paper presents neutron diffraction and contour method results, and compares these experimental stress measurements to a WRS Finite Element (FE) model. Finally details are provided on the procedure used to calculate the residual stress distribution in the restrained or as welded condition in order to allow comparison to other residual stress data collected as part of Phase 1 of the WRS program.

## INTRODUCTION

Pressurized water reactor piping system dissimilar metal welds are susceptible to Primary Water Stress Corrosion Cracking (PWSCC) as an active degradation mechanism. PWSCC is highly influenced by the state of stress within susceptible material with tensile residual stresses in welds being an established driving force for PWSCC. Proper predictions or measurements of these residual stresses are essential to accurate crack initiation and growth assessment. The NRC and EPRI are working cooperatively under a memorandum of understanding

to validate weld residual stress prediction in pressurized water reactor primary cooling loop components containing dissimilar metal (DM) welds [1-3]. This paper focuses on the characterization of residual stress in a lab sized plate specimen (P4) from Phase 1 of the NRC/EPRI WRS program, where specimens were designed to partially mock up DM welds typical of pressurized water reactor primary piping system loops. Later phases of the programs studied full scale pressurizer surge nozzle mock ups (Phase 2) and explant material gathered from canceled plants (Phase 3, 4).

Welding residual stresses, particularly in DM welds, present several challenges to experimental measurement techniques. Elastic release techniques (contour method and hole drilling) are prone to artifact in regions of high residual stress as a result of plasticity at the measurement location, while diffraction based techniques can be very sensitive to changes in local chemistry at the DM weld interface. Therefore the results from the three measurement techniques are compared with each other and to a finite element model of the welding process. Characterization of this plate specimen was different than other data collected as part of the Phase 1 characterization effort, as the plate was removed from its restraint prior to conducting residual stress measurements. In order to compare with other results of the study, this paper details a correction procedure and all results presented herein reflect the restrained or as welded condition.

## WELD GEOMETRY

<sup>1</sup> Matthew Kerr is now at the Knolls Atomic Power Lab and can be reached at [matthew.kerr.contractor@unnpp.gov](mailto:matthew.kerr.contractor@unnpp.gov).

<sup>2</sup> The views expressed herein are those of the authors and do not represent an official position of the U.S. NRC or Los Alamos National Lab.

All Phase 1 plate specimens were fabricated by Edison Welding Institute (EWI) using an automated gas tungsten arc welding (GTAW) procedure, depositing Alloy 82 weld metal in a machined groove on an annealed 304L SS plate [4, 5]. Nominal plate dimensions were 203 mm x 356 mm x 15.25 mm with a trapezoidal groove 10.15 mm in depth (groove root is 8.64 mm with an opening angle of 60°). 7 weld passes were deposited for the P4 plate with identical torch conditions (225 A, 11.5 V, and a travel speed of 1.5 mm/s) with all weld passes starting on the same side of the plate. Restraint was applied during welding by an aluminum backing plate loaded by bevel washers with linear force/displacement behavior with weld and restraint geometry illustrated in Figure 1. During welding thermocouple data was collected and bead geometry was measured using laser profilometry between passes. Residual stress measurements discussed below were conducted on a longitudinal plane approximately mid-way between 2 previous measurement locations 180 mm apart conducted as part of the EPRI led residual stress characterization (specifically a ring core measurement and stress-free reference comb from a previous neutron measurement), see Figure 1b.

## NEUTRON MEASUREMENT

Neutron Diffraction (ND) measurements were conducted at the SMARTS instrument at the Los Alamos Neutron Science Center (LANSCE) [6]. Measurement locations are indicated by the black diamonds in Figure 2 using a gage volume of 2 mm x 2 mm x 6 mm defined by incident slits and radial collimators. Two orthogonal scattering geometries were used in order to measure the three principle plate stress components [6, 7]. The count time for each measurement location varied from 20 to 120 minutes depending on the amount of nickel in the neutron path length, with count time optimized based on minimizing lattice parameter refinement uncertainty (indicating a stable peak-to-background ratio had been achieved). The chemistry gradient of iron and nickel across the dissimilar metal weld/heat affected zone necessitated characterization of the stress-free lattice parameter at each measurement location, as apparent strains of  $\sim 3000 \mu\epsilon$  (or stresses of  $\sim 1$  GPa) resulted from chemistry variation across the weld/heat affected zone. Stress-free lattice parameter measurements were made on a comb with teeth 3.5 mm x 3.5 mm in cross section and used to calculate lattice strain at each measurement location. The comb was harvested from the measurement plane after completion of the contour method measurement described in the next section. Diffraction patterns were analyzed using a full-pattern Rietveld analysis, where the all available diffraction peaks are simultaneously refined to an average lattice parameter [8]. The use of average lattice parameter allows lattice strains calculated to be compared to continuum mechanics strains, residual stresses is then directly calculated using Hooke's law and elastic modulus appropriate for bulk material (in this case, 195 GPa for the 304L and 205 GPa for the Alloy 82) [7, 9]. Longitudinal stresses measured with neutron diffraction are plotted in Figure 2(a).

## CONTOUR METHOD MEASUREMENT

Contour method measurement of the P4 plate was conducted at LANL in order to measure the longitudinal stress in the weld at the same location as the neutron diffraction measurements. The measurements followed standard procedures for the contour method [11]. The sectioning cut for the contour method measurement was made using wire electric discharge machining (EDM) with a 100  $\mu\text{m}$  diameter brass wire and skim-cut settings in order to minimize stresses induced by the cutting process [10]. The plate was clamped on both sides in order to minimize deformation and possible cutting artifact as the stresses relaxed during the sectioning operation. Following completion of the sectioning operation profilometry of each sectioned surface was conducted on a 0.5 mm grid using a coordinate measuring machine equipped with a 1 mm diameter touch probe [11]. The surfaces were low in the weld region with peak-to-valley surface heights of 135  $\mu\text{m}$  and 165  $\mu\text{m}$  on the two sections. Raw coordinate data was processed using smoothed quadratic splines achieving approximately millimeter spatial resolution [11, 12]. The smoothed surface displacement data was mapped onto 3D meshes of each plate section using reduced-integration bi-quadratic (20 node) hexahedral elements in Abaqus (C3D20R) [14]. Plate sections were not symmetric as a result of previous plate characterization, and these differences were accounted for in the contour FE in order to avoid potential artifacts resulting from different plate stiffness for each section. Residual stresses were then calculated using an elastic FE analysis based on the measured surface displacements and bulk elastic modulus values used in the previous section, results from each plate section were averaged together. Longitudinal stresses measured with the contour method are plotted in Figure 2(b). After the measurements, a stress-free test cut was made by cutting a 1 mm slice off of the cut surface of one section. The contour from the test cut was flat to within a few microns, which validates the assumption of constant cut width [15]

## SURFACE HOLE DRILLING MEASUREMENT

After completion of the contour method measurements surface residual stress measurements using hole drilling were conducted at LANL in the larger of the two sectioned plate sections, and reported in the longitudinal and transverse directions. The hole drilling set up used Electronic Speckle Pattern Interferometry (ESPI) to measure surface deformation rather than the strain gages typically used in a conventional hole drilling set up. Using ESPI strain is measured by illuminating on optically rough surface with constant wavelength light to generate an interference pattern. The deformation is used to calculate stresses using the elastic constants previously assumed. A complete description of the ESPI set-up and calculation method used in this work is found in the following reference [16].

Holes were drilled in the plate surface to a depth of 0.32 mm using a 1.6 mm diameter double fluted square end mill driven by an electric spindle rotating at 40,000 revolutions per minute.

Residual stress results are reported at 0.16 mm (one half of the hole depth), assuming that there is little stress with depth gradient in the plate. Hole drilling measurements were made in columns transverse to the weld; each column comprised 8 individual measurements, consisting of three holes symmetrically located on each side of the weld and two holes in the weld material. A total of five columns of measurements were made, with spacing of 0.375" between columns. To obtain some quantification of the repeatability of the measurements, multiple measurements were made at the same distance from the weld center in columns 1, 3, and 5. To provide good resolution and still maintain a distance of 9.5 mm (5 hole diameters), the measurement locations of columns 2 and 4 were offset by approximately 5 mm from those of 1, 3 and 5. (This guideline for hole positioning was deviated in the area of the weld material out of necessity due to measurement difficulty on the uneven surface of the weld.) The spacing and stress results are shown for each column in Table 1; the values shown are after correction for the bending stress induced by the clamping device, as discussed in the section on Clamp Correction. Measured stresses at a given distance to the weld were averaged and are shown in the plots of Figure 5b and 6b. The uncertainty of hole drilling measurements of this type is typically  $\pm 25$  MPa [16], and the variation indicated between measurements at equal distance from the weld supports this level of uncertainty.

## FINITE ELEMENT WRS MODEL

To model the residual stress distribution, the heat flow and mechanical deformation during welding were simulated using a 2D decoupled FE WRS model in Abaqus. In a decoupled approach, first the transient heat-transfer analysis is conducted to solve the temporal and spatial distribution of the temperature in the model. This temperature distribution is then mapped to a generalized plane strain mechanical analysis to calculate the residual stress field. Temperature dependent thermal/mechanical properties, melting, solidification, and annealing were accounted for in the analysis. A pass-by-pass weld simulation was performed, where a weld pass is activated when deposited and heat transfer is assumed to occur on all free surfaces of the model. Bead geometry from laser profilometry was used to construct the mesh of the weld region. The welding arc was modeled using a 1D formation of the Goldak double-ellipsoidal heat source, effectively applying the heat source simultaneously over the length of the weld [17, 18]. The weld model used in this work is similar to those used thick section welds studied as part of the NRC/EPRI WRS Program [1, 2]. Material properties used are those released with the Phase 2 International Round Robin FE modeling package [2], which are very similar to those used in the British Energy dissimilar metal weld work program [19].

Two thermal models were conducted as part of this work. The first model assumed convective heat transfer occurred equally on all surfaces of the plate. Torch efficiency was adjusted (between 40 and 65%) to match the peak temperature from thermocouple (TC) data and fully melt the weld beads as identified by the weld macrograph in Figure 3. This approach had reasonable agreement with peak temperature for TC1, TC locations are illustrated in Figure 3, but over predicted temperatures at TC2/3 as the heat removed by the backing plate was not accounted for by the convective surface modeled. To account for conductive heat removal along the backing plate the convection coefficients on this surface were increase by a factor of 25, allowing peak temperature, heat removal, and fusion area to be captured using a 70% welding torch efficiency for all 7 passes as show in Figure 3. Residual stress profiles calculated from each thermal model are similar in magnitude and only results from the second thermal model (higher heat removal on plate back) will be discussed below.

For the mechanical model, material properties were assigned from the Phase 2 modeling package for the 304L SS plate and Alloy 82 weld metal. Hardening behavior of annealed austenitic steels is similar [21] and 316 SS properties from the Phase 2 modeling package were assumed for the annealed 304L plate. Yield and ultimate tensile stress values for the 304L plate were with 5% of the room temperature 316 SS values [4]; therefore material properties were not scaled. The choice of hardening law has been identified as one of the major sources of variability in WRS simulations in several recent studies [1, 2, 19, 22]. All source material properties were all in the annealed condition, therefore isotropic hardening represents an upper bound stress estimate and the linear kinematic is a lower bound stress estimate. While the linear kinematic hardening represents lower bound, it is not a conservative lower bound estimate on stress [22] and linear kinematic results are reported as these results tend to envelope the experimental data collected. Spring loaded analytically rigid surfaces were used to account plate restraint during welding. Load displacement behavior of the bevel washers was distributed in the Phase 1a modeling package [4] and the stiffness of the spring elements in the 2D model was adjusted to account for the total number of bevel washers used per side at a single location on each analytic surface. Prior to welding spring elements were also loaded based on the initial displacements recorded in the Phase IA modeling package [4]. Longitudinal stress results from the WRS FE model are plotted in Figure 2(c).

## CLAMP CORRECTION

The P4 plate characterized in this study was removed from the restraint to in order to facilitate neutron diffraction measurements and reduce uncertainty during contour method measurements. In order to compare with other measurements in the study, the effect of removing the restraints had to be modeled. During removal from the restraint the P4 plate was

strain gaged at two locations 12.7 mm from the edge of the weld on the top surface of the plate. Stresses relaxed by removal from the restraint were calculated using a 3D FE model (LANL) to mimic the actual constraints. For the starting geometry, the 3D FE model used the plate perimeter measured during the contour method profilometry. Displacement boundary conditions used to model the clamping were adjusted to match the experimentally measured strain gage readings on the plate surface (yielding a stress uncertainty of  $\pm 10\%$ ). All restraint components are accounted for in the clamping analysis (aluminum backing plate and steel clamps). Figure 4 plots longitudinal and transverse correction components along the indicated line ( $Y = 6\text{ mm}$ ). Analysis assumes that all plate deflection is elastic and that the stresses relaxed by the clamping process can be directly added to the unclamped experimental residual stress results, allowing comparison with data collected as part of the EPRI lead Phase 1 WRS program. Along the plate neutral axis or mid-plane ( $y = 0\text{ mm}$ ) no correction is required, but away from the mid-plane the transverse correction is a function of position. The transverse (bending) stress component was most affected by the correction, while the stresses longitudinal to the weld showed a small, but noticeable, correction.

The plate perimeter measured during the contour method measurement and plotted in *Figure 4(a)* is different than the unclamped plate profile predicted in the 2D WRS FE model, likely a result of the simultaneous heat input across the weld bead in the 2D WRS FE model. The 2D WRS FE model does not account for the shape change of the plate, potentially underestimating both plate deflection and the transverse stress components away from the mid-plane. In order to capture this effect a 3D WRS FE model was constructed using the decoupled approach previously described. Rather than apply the heat input simultaneously through thickness, each weld bead was divided into 5 regions or blocks and the heat input was applied sequentially to each of the 5 blocks. Heat input was similar to the 2D model, as confirmed by the temperature profiles and metallographic comparison. The unclamped 3D WRS FE plotted in *Figure 4(b)* show good agreement with the perimeter measured during the contour method measurements and the transverse stresses near the outer surface of the plate ( $y = 6\text{ mm}$ ) show a 1:1 agreement with the clamped 2D WRS FE results. This suggests that both the 2D and 3D WRS FE models have the same total bending moment on the plate as a result of the restraint, despite the differences observed between the unclamped 2D and 3D plate profile.

While the 2D and 3D WRS FE results show similar restrained transverse stress profiles, the clamp corrected experimental data plotted in *Figure 5(b)* is consistently high with respect to the WRS FE. One possibility is that the WRS FE is underestimating the total restraint on the plate during welding, though this seems unlikely as the measured plate profile is in good agreement with the unclamped 3D WRS FE plate profile. The other possibility is that the strain gages are sensitive to

plasticity at the plate surface during unclamping, producing a correction that is too high as the stress relaxation is assumed elastic. The transverse stresses are most sensitive to this artifact, as the transverse stresses at the outer surface are closest to yield. The longitudinal stress correction is smaller in magnitude and largely insensitive to the restraining load applied. Therefore the comparison of the longitudinal WRS FE model results to experimental measurements is conducted at all measurement locations, while the transverse/normal stress components are only compared along the plate mid-plane (where the bending moment from clamping is zero).

## COMPARISON OF RESULTS

Longitudinal stress results have been compared along the scan lines conducted for neutron diffraction using the plate mid-plane ( $y = 0\text{ mm}$ ) and centerline ( $x = 0\text{ mm}$ ) as a reference. For the mid-plane locations both neutron diffraction and contour results show a similar trend, compressive stresses at the plate edges with tensile stresses peaking in the plate center (*Figure 6(a)*). Similar trend is shown for the  $y = 6\text{ mm}$  scan line, though the stress magnitudes for the neutron and contour data are in better agreement (*Figure 6(b)*), and corroborated by the hole drilling results. The hole drilling measurements in the region of the weld show a significantly lower magnitude of stress in both the transverse and longitudinal direction than the other measurements and the FE predictions, which is unexplained at this time. In general, neutron results tend to be higher in magnitude than the contour results and the stresses peak over a broader region of the weld. FE WRS results bound the experimental results in the weld, with the isotropic hardening a better correlation to the neutron data and the kinematic hardening a better correlation to the contour results.

In addition to the longitudinal comparison, neutron diffraction data for the normal and transverse stress components have been compared to the FE WRS model results along the weld mid-plane (*Figure 7*). Normal stresses are expected to be low in magnitude as the plate thickness is relatively low when compared to the other dimensions. Transverse stresses are also expected to be relatively low as the bending stresses should cancel along the weld mid-plane. The magnitude of FE WRS model and neutron data is similar, but opposite in sign in the weld region. FE WRS model shows both longitudinal and normal stress components compressive in the weld, while the neutron diffraction shows these components in tension. Neutron results show tension in all three stress components in this region, suggesting that perhaps the stress-free reference parameter is not completely free of chemistry artifacts.

In the scans parallel to the weld centerline ( $x = 0\text{ mm}$ ,  $-3.5\text{ mm}$ ,  $-7\text{ mm}$ ,  $-10.5\text{ mm}$ ) the effect of the weld/base metal interface is more pronounced in the neutron data. *Figure 8* shows that at the weld/base metal interface (points with unfilled symbols), neutron results are systematically high and these points are excluded from further comparison. Along the weld centerline,

neutron diffraction data are more scattered and trend lower than contour results (Figure 8 (a)). Away from the weld centerline ( $x = -3.5$  mm,  $-7$  mm,  $-10.5$  mm in Figure 8 (b-d)), the comparison is more favorable showing similar stress profile and magnitudes to the contour results. The FE WRS results with isotropic hardening show a similar stress profile to the experimental data, though in all cases stresses are higher with respect to the experimental data and the comparison tends to improve away from the weld centerline. As a point of reference, results using the mixed hardening from the British Energy work package fall somewhat close to the isotropic upper bound estimate illustrated in Figure 8 (a) [19].

In the weld, fitting uncertainty on the neutron data appears smaller than the realized uncertainty. The steep gradient in chemistry and microstructure in the weld region makes the realized uncertainty difficult to quantify. The observed scatter in peak intensity plotted in Figure 9 suggests point-to-point counting statistics variation in the weld is limiting the realized strain resolution, as the apparent center of the diffraction volume varies from point-to-point [7].

Because of the difficulty of measuring residual stresses, using at least two techniques that have different assumptions serves as a check on the accuracy of experimental results. Unfortunately, in this study, the neutron and contour method results did not agree very well, making it difficult to use the results to make detailed conclusions about the finite element model. It is difficult to assess which results might be more accurate. In specimens other than fusion welds, contour method measurements usually agree quite well with neutron diffraction or synchrotron diffraction measurements [12, 13, 23, 24]. In fusion welds, the agreement is sometimes quite good [25, 26] but often the agreement is not very good [27, 30]. Both methods have errors that could affect measurements in welds. Neutron diffraction is sensitive to chemistry and microstructure variations [31], and the large variations of stress-free lattice parameter in the P4 specimen are consistent with that issue. When the stresses are quite large, the contour method can be affected by errors in the cut width assumption [15] or by plasticity errors during the stress relaxation [32, 33]. The hole drilling results in Figure 5b agree well with neutron diffraction results, but only in the region away from the weld. The neutron diffraction results were carefully corrected for chemistry variations by using reference samples taken from the same location as the stress measurements. Nonetheless, the scatter in results near the weld, including a peak value of over 800 MPa in Figure 8 decrease confidence in the results near the weld interface where the chemistry variation is the greatest.

## CONCLUSIONS

The following conclusions can be drawn from this work:

- Longitudinal stresses measured with neutron diffraction and contour method show good agreement at locations

away from the weld centerline ( $x = 0$  mm) and excluding neutron measurement locations at the weld base metal interface. Stress profiles measured parallel to the weld mid-plane with neutron diffraction tend to be broader and higher in magnitude than those measured with the contour method.

- WRS FE simulations using input material properties in the annealed condition, effectively bound the experimental results assuming isotropic and linear kinematic hardening. The lack of agreement between the different measurements made it difficult to assess which modeling variations would be more accurate.
- Residual stress measurements were made in the unrestrained state and details of a correction were provided in order to allow comparison to residual stress data collected as part of EPRI lead Phase 1 WRS program.
- Analysis conducted in support of the correction factor highlighted the geometric sensitivity of the restraint used, allowing limited comparison of the experimental data and FE WRS model results.

## ACKNOWLEDGMENTS

The authors would like to thank John Broussard (Dominion Engineering Incorporated) and Paul Crooker (EPRI) for providing the plate specimen used in this characterization effort.

## REFERENCES

1. M Kerr, HJ Rathbun, 2012, "Summary of Finite Element (FE) sensitivity studies conducted in support of the NRC/EPRI Welding Residual Stress (WRS) program," in Proceedings of ASME Pressure Vessels and Piping Conference, PVP2012-78883, Toronto, ON Canada.
2. LF Fredette, M Kerr, HJ Rathbun, J Broussard, 2011, "NRC/EPRI welding residual stress validation program – phase III details and findings," in Proceedings of the ASME Pressure Vessels and Piping Conference, PVP2011-57645, Baltimore, MD.
3. Addendum to the Memorandum of Understanding (MOU) between NRC's Office of Nuclear Regulatory Research and Electric Power Research Institute, Inc. on Cooperative Nuclear Safety Research", NRC ADAMS Accession Number ML103490002, 2/15/2011
4. J Broussard, 2009, "Fabrication of Phase 1A Weld Specimens for EPRI Welding Residual Validation Project," in Phase 1A modeling package, prepared by Dominion Engineering, Inc., DEI project number S-5572-00-02-1.
5. S Levesque, 2008, "Plate Welds for Residual Stress Validation," in Phase 1A modeling package, prepared by Edison Welding Institute, EWI project number 51450CSP.

6. MAM Bourke, DC Dunand, E Ustundag, 2002, "SMARTS – a spectrometer for strain measurement in engineering materials," *Applied Physics A Materials Science Processing*, **74**, pp. 1707-1709.
7. MT Hutchings, PJ Withers, TM Holden, T Lorentzen, 2005, Introduction to the characterization of residual stress by neutron diffraction, CRC Press.
8. RB Von Dreele, JD Jorgensen, CG Windsor, 1982, "Rietveld refinement with spallation neutron powder diffraction data," *Journal of Applied Crystallography*, **15**, pp. 581-589.
9. MR Daymond, 2004, "The determination of a continuum mechanics equivalent elastic strain from the analysis of multiple diffraction peaks," *Journal of Applied Physics*, **96**, 4263.
10. W Cheng, I Finnie, M Gremaud, MB Prime, 1994, "Measurement of near-surface residual-stresses using electric-discharge wire machining," *Journal of Engineering Materials Technology*, **116**, pp. 1-7
11. MB Prime, RJ Sebring, JM Edwards, DJ Hughes, PJ Webster, 2004, "Laser surface-contouring and spline data-smoothing for residuals stress measurement," *Experimental Mechanics*, **44**, pp. 176-184.
12. P Pagliaro, MB Prime, H Swenson, B Zuccarello, 2009, "Known residual stress specimens using opposed indentation," *Journal of Engineering Materials Technology*, **116**, pp. 1-7.
13. P Pagliaro, MB Prime, JS Robinson, B Clausen, H Swenson, M Steinzig, and B Zuccarello, 2011, "Measuring inaccessible residual stresses using multiple methods and superposition," *Experimental Mechanics*, **51**, pp. 1123-1134
14. Abaqus 6.10, Dassault Systèmes Simulia Corp., Providence, RI, USA, 2010.
15. M. B. Prime, A. L. Kastengren, 2010, "The Contour Method Cutting Assumption: Error Minimization and Correction" Proceedings of the SEM Annual Conference & Exposition on Experimental and Applied Mechanics Indianapolis, Indiana USA, Society for Experimental Mechanics Inc., June 7 - 9, 2010, paper # 507
16. M. Steinzig, E. Ponslet, 2003, "Residual stress measurements using the hole drilling method and laser speckle interferometry-Part I," *Experimental Techniques*, **27**.
17. JA Goldak, M Akhlaghi, 2005, Computational Welding Mechanics, Springer.
18. Y Chen, D Rudland, G Wilkoski, 2004, "Impact of welding sequence of the CRDM nozzle-to-vessel weld stress analysis," in Proceedings of ASME Pressure Vessels and Piping Conference, PVP2004-2556, San Diego, CA.
19. FW Brust, T Zhang, D-J Shim, S Kalyanam, G Wilkowski, M Smith, A Goodfellow, 2010, "Summary of weld residual stress analyses for dissimilar metal weld nozzles," in Proceedings of the ASME Pressure Vessels and Piping Conference, PVP2010-26106, Bellevue, WA.
20. T Zhang, FW Brust, G Wilkowski, 2012, "Weld residual stress in various large diameter nuclear nozzles," *Journal of Pressure Vessel Technology* (in press).
21. AF Armas, OR Bettin, I Alvarez-Armas, GH Rubiolo, 1988, "Strain aging effects on the cyclic behavior of austenitic stainless steels," *Journal of Nuclear Materials*, **155-157**, pp. 644-649
22. MC Smith, O Muránsky, PJ Bendeich, L Edwards, 2010, "The impact of key simulation variables on predicted residual stresses in pressurizer nozzle dissimilar metal weld mock-ups. Part 1 – Simulation," in Proceeding of the ASME Pressure Vessels and Piping Conference, PVP2010-26023, Bellevue, WA.
23. A Evans, G Johnson, A King, and PJ Withers, 2007, "Characterization of laser peening residual stresses in AL 7075 by synchrotron diffraction and the contour method," *Journal of Neutron Research*, **15**, pp. 147-154.
24. RJ Moat, AJ Pinkerton, L Li, PJ Withers, M Preuss, 2011, "Residual stresses in laser direct metal deposited Waspaloy," *Materials Science and Engineering: A*, **528**, pp. 2288-2298.
25. Y Zhang, S Ganguly, L Edwards, ME Fitzpatrick, 2004, "Cross-sectional mapping of residual stress in a VPPA weld using the contour method," *Acta Materialia*, **52**, pp. 5225-5232.
26. ME Kartal, CDM Liljedahl, S Gungor, L Edwards, ME Fitzpatrick, 2008, "Determination of the profile of the complete residual stress tensor in a VPPA weld using the multi-axial contour method," *Acta Materialia*, **56**, pp. 4417-4428.
27. PJ Withers, M Turski, L Edwards, PJ Bouchard, DJ Buttle, 2008, "Recent advances in residual stress measurement," *The International Journal of Pressure Vessels and Piping*, **85**, pp. 118-127.
28. D Thibault, P Bocher, M Thomas, M Gharghoury, M Côté, 2010, "Residual stress characterization in low transformation temperature 13%Cr-4%Ni stainless steel weld by neutron diffraction and the contour method," *Materials Science and Engineering: A*, **527**, pp. 6205-6210.
29. DW Brown, TM Holden, B Clausen, MB Prime, TA Sisneros, H Swenson, J Vaja, 2011, "Critical Comparison of Two Independent Measurements of Residual Stress in an Electron-Beam Welded Uranium Cylinder: Neutron Diffraction and the Contour Method," *Acta Materialia*, **59**, pp. 864-873.
30. F Hosseinzadeh, MB Toparli, PJ Bouchard, 2012, "Slitting and Contour Method Residual Stress Measurements in an Edge Welded Beam," *Journal of Pressure Vessel Technology*, **134**, pp. 011402-011406.
31. TM Holden, H Suzuki, DG Carr, MI Ripley, B Clausen, 2006, "Stress measurements in welds: Problem areas," *Materials Science and Engineering: A*, **437**, pp. 33-37.

32. SH Shin, 2005, "FEM analysis of plasticity-induced error on measurement of welding residual stress by the contour method," *Journal of Mechanical Science and Technology*, **19**, pp. 1885-1890.
33. RJ Dennis, DP Bray, NA Leggatt, M Turski, 2008, "Assessment of the influence of plasticity and constraint on measured residual stresses using the contour method," in *Proceedings of the ASME Proc. 2008 ASME Pressure Vessels and Piping Conference*, PVP2008-61490, Chicago, IL.

## Figures

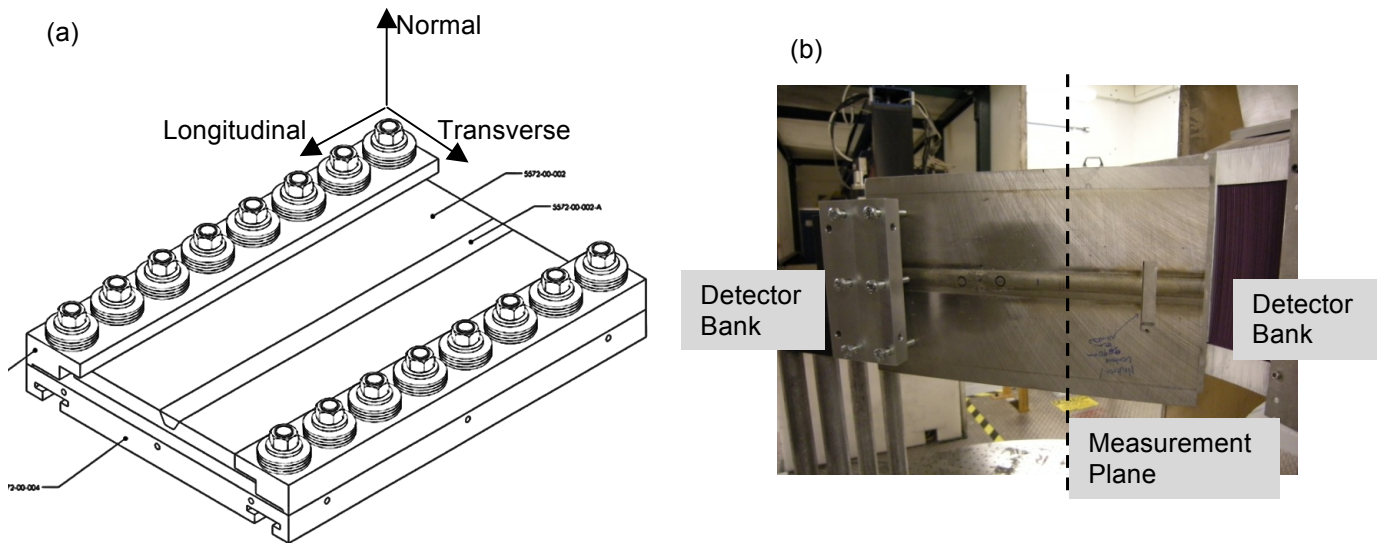


Figure 1 – Schematic of the P4 plate specimen and restraining clamp (a) drafting showing axis convention used and (b) measurement location and neutron scattering geometry for the longitudinal/normal strain components.

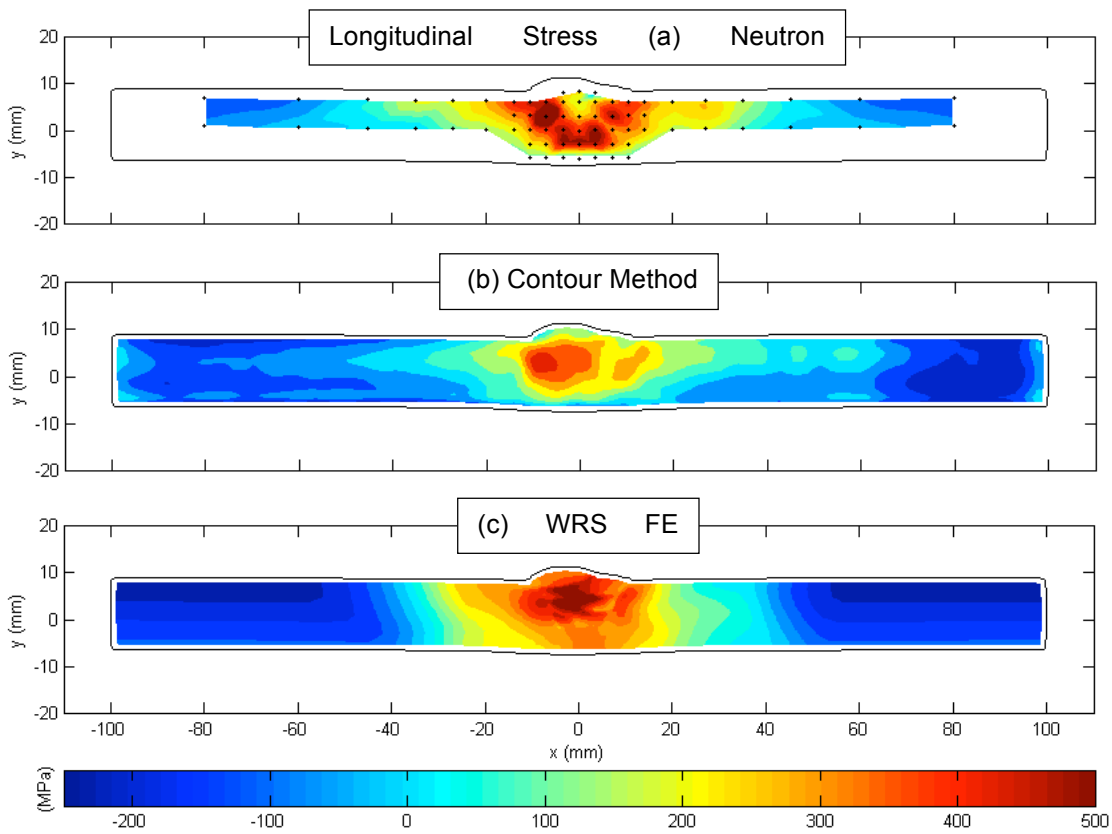


Figure 2 – Comparison of longitudinal stresses in the restrained or as welded condition (a) neutron diffraction with black diamonds indicating the measurement location, (b) contour method, and (c) WRS FE model results using isotropic hardening. Plate perimeter as measured in the contour method is plotted as a point of reference.

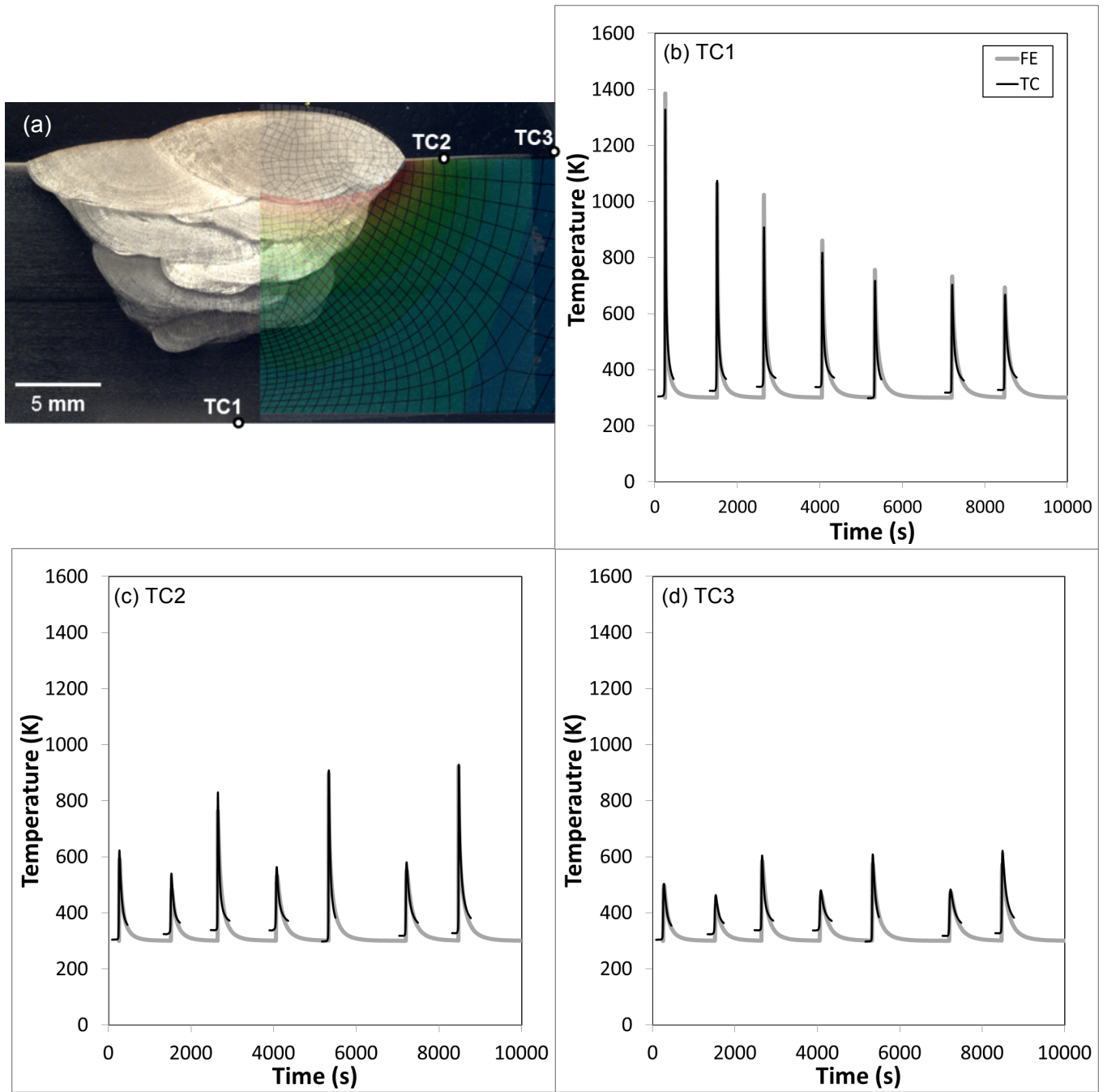


Figure 3 – Results from WRS FE thermal model (a) comparison of the fusion zone to weld macrograph, (b-d) TC data vs. WRS FE thermal model.

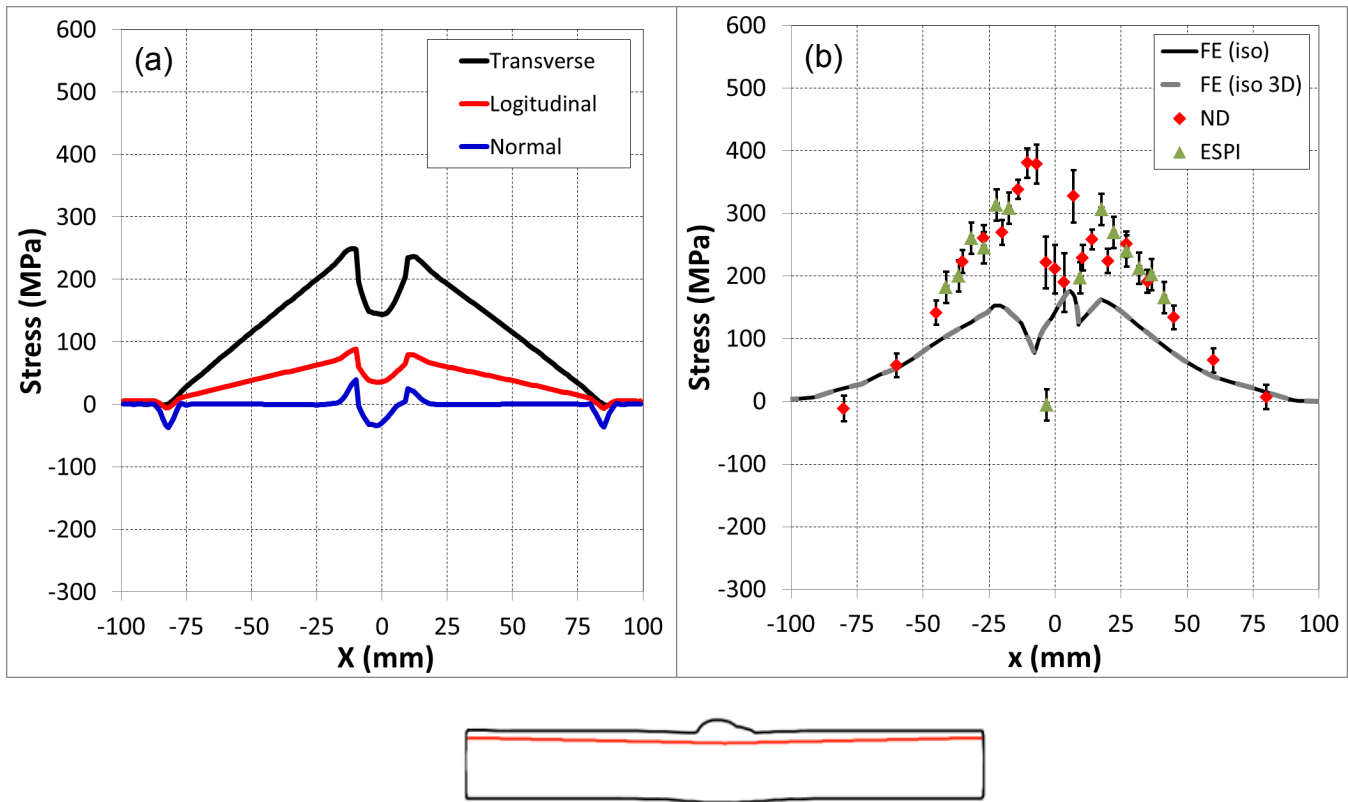


Figure 4 – (a) Calculated correction factors along the indicated line ( $y = 6 \text{ mm}$ ), transverse correction is the most significant. And (b) correction over corrects the residual stress data relative to the FE calculations.

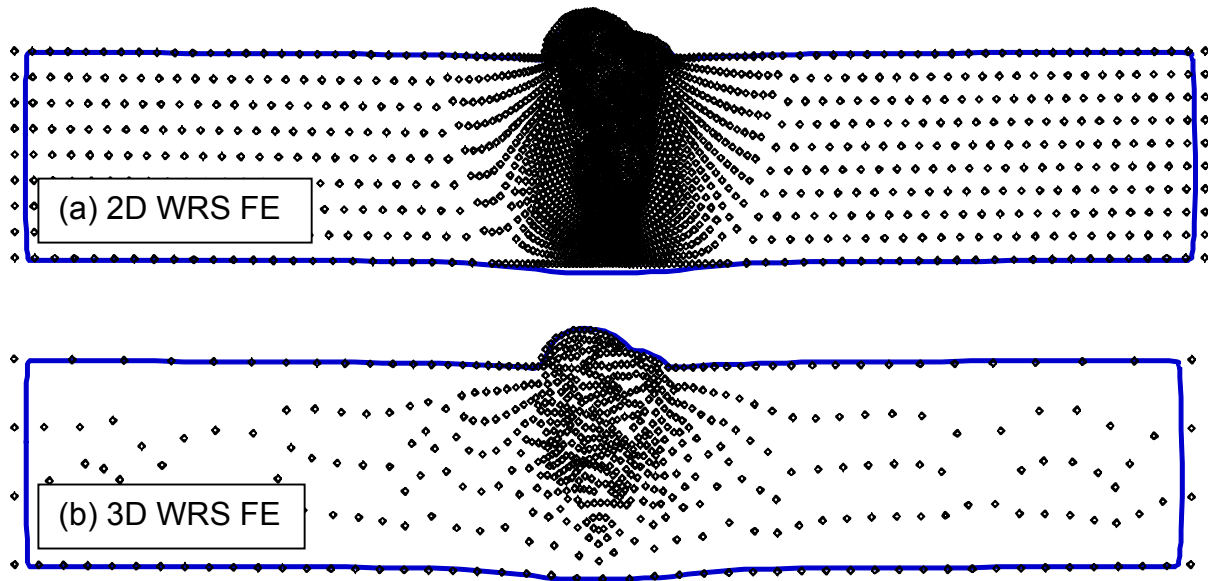


Figure 5 – Comparison of unrestrained plate perimeter (solid line) as measured from the contour method profilometry to (a) 2D and (b) 3D WRS FE model (diamonds).

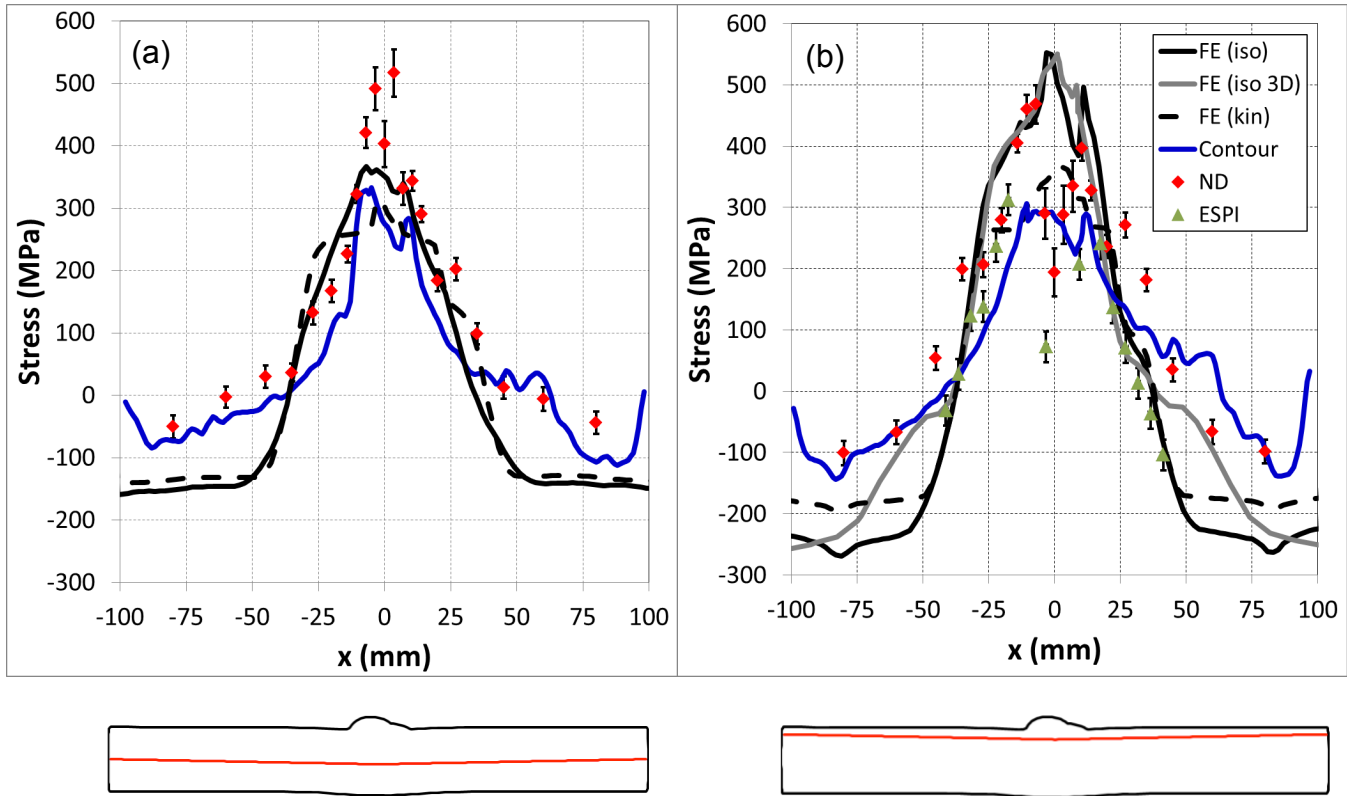


Figure 6 – Comparison of longitudinal stresses at (a) mid-plane ( $y = 0$  mm) and (b) parallel to the mid-plane ( $y = 6$  mm).

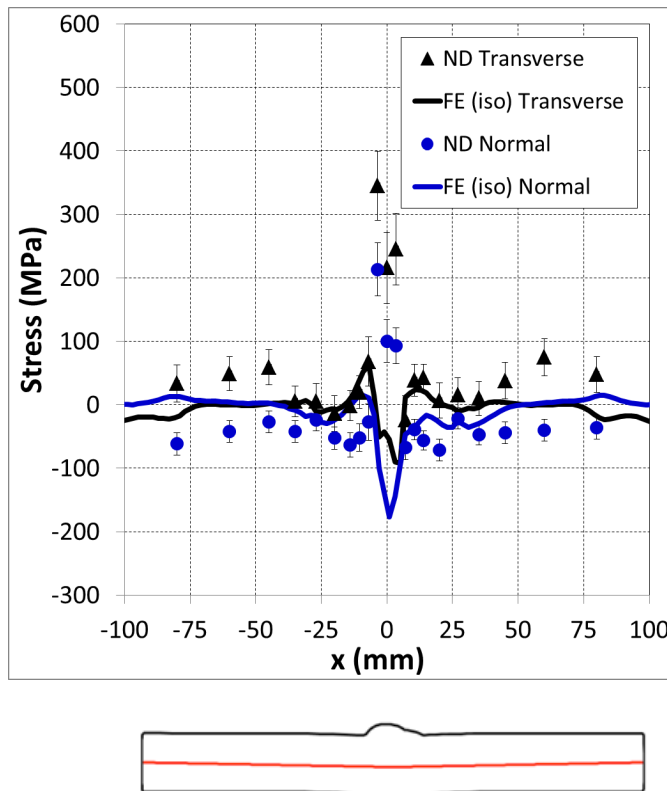


Figure 7 – Comparison of transverse and normal stress components at mid-plane

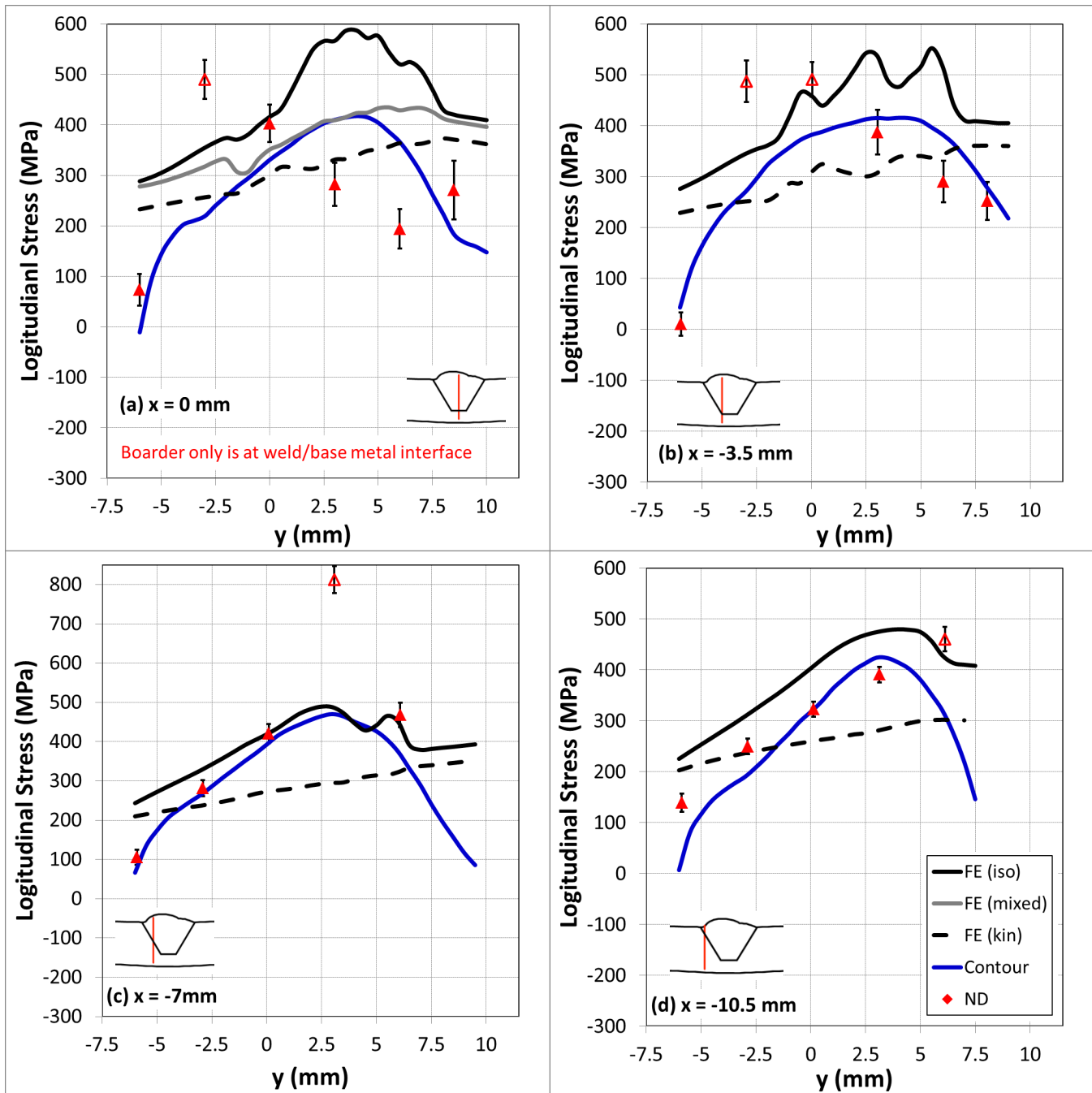


Figure 8 – Comparison of longitudinal stress components along (a) centerline,  $x = 0$  mm, (b)  $x = -3.5$  mm, (c)  $x = -7$  mm, and (d)  $x = -10.5$  mm. Same color convention as Figure 6 is followed, grey line in (a) results from a WRS FE model using the mixed hardening law from the British Energy work package [19].

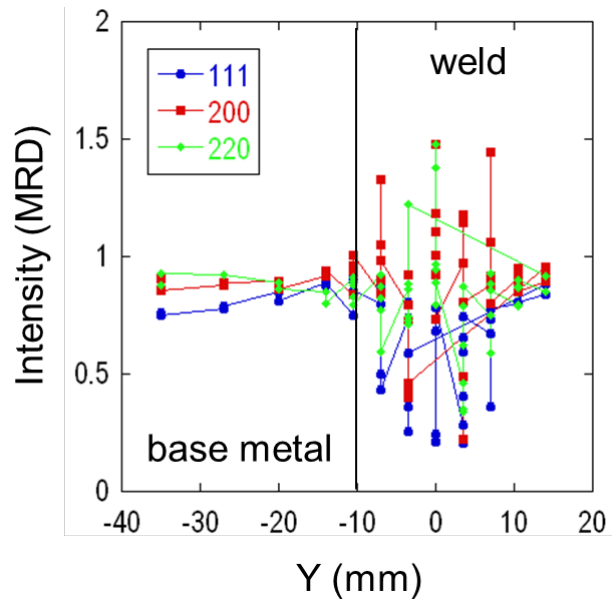


Figure 9 – Peak intensity as a function of weld position, showing that point-to-point intensity variation is greater in the weld than in the base metal.